Mon. Not. R. Astron. Soc. , 1–10 (2001) Printed 1 February 2008 (MN LATEX style file v1.4)

Spectral variability in transonic discs around black holes

Luca Zampieri[1], Roberto Turolla[1] and Ewa Szuszkiewicz[1,2,3,4]
[1] *Department of Physics, University of Padova, via Marzolo 8, 35131 Padova, Italy*
[2] *Institute of Physics, University of Szczecin, ul. Wielkopolska 15, 70-451 Szczecin, Poland*
[3] *Torun Centre for Astronomy, Nicolaus Copernicus University, ul. Gagarina 11, 87-100 Toruń, Poland*
[4] *International School for Advanced Studies, via Beirut 2-4, 34013 Trieste, Italy*

1 February 2008

ABSTRACT
Transonic discs with accretion rates relevant to intrinsically bright Galactic X-ray sources ($L \approx 10^{38}$–10^{39} erg s^{-1}) exhibit a time dependent cyclic behaviour due to the onset of a thermal instability driven by radiation pressure. In this paper we calculate radiation spectra emitted from thermally-unstable discs to provide detailed theoretical predictions for observationally relevant quantities. The emergent spectrum has been obtained by solving self-consistently the vertical structure and radiative transfer in the disc atmosphere. We focus on four particular stages of the disc evolution, the maximal evacuation stage and three intermediate stages during the replenishment phase. The disc is found to undergo rather dramatic spectral changes during the evolution, emitting mainly in the 1–10 keV band during outburst and in the 0.1–1 keV band off-outburst. Local spectra, although different in shape from a blackbody at the disc effective temperature, may be characterized in terms of a hardening factor f. We have found that f is rather constant both in radius and in time, with a typical value ~ 1.65.

Key words: accretion, accretion discs – black hole physics – instabilities – radiative transfer

1 INTRODUCTION

Observations of Galactic black hole candidates (BHCs) and active galactic nuclei (AGNs) have gone a long way in obtaining very detailed information on these sources. The analysis of X-ray data revealed the existence of at least four distinct spectral states in BHCs, defined on the basis of the spectral shape and the flux level (see e.g. Tanaka & Lewin (1995); Narayan, Mahadevan & Quataert (1999) for reviews). In the high (soft) state the spectrum is dominated by a soft thermal component, commonly attributed to a standard accretion disc. In the low (hard) state a power-law high energy tail, probably originated by the comptonization of soft photons by a hotter medium, dominates the spectrum. Usually, as the flux decreases, the power-law component becomes more and more pronounced, while the thermal one weakens and eventually disappears. Optical/UV/X-ray AGN spectra consist of three main components: a big blue bump, a soft X-ray excess, a hard power-law tail with a reflection hump and a high-energy cut-off (see e.g. Zdziarski et al. (1996) for a review). As it was realized long ago, by shifting a typical AGN spectrum to higher energies by a factor ≈ 100, such that the big blue bump falls in the 1-10 keV band, one obtains a X-ray spectrum which closely resembles that of a typical BHC in an intermediate state. The actual similarity between these two classes of sources (modulo the energy shift) is corroborated by a number of observational evidences (see e.g. Grebenev et al. (1993); Grebenev, Sunyaev & Pavlinsky (1997) for the properties of power-law tails and Zdziarski, Lubiński & Smith (1999) for the spectral index-Compton reflection hump correlation).

In the last few years, a great wealth of information on the physical conditions in BHCs has come from the study of their variability. Besides transitions among different spectral states (on time-scales $\approx$ 1 hour-1 month), time analysis revealed much more rapid variations, ranging from very low (mHz) to high-frequency (100 Hz) QPOs. In some sources (e.g. GRS 1915+105) phase lags between photons in different X-ray bands have been detected, with typical values in the range 10-1000 ms (Cui et al. (1999); Reig et al. (2000); Cui, Zhang & Chen (2000); Pottschmidt et al. (2000)). If the characteristic times scale linearly with the black hole mass, as one naively expects, the shortest variability in AGNs should occur on $\sim$ hours-days. Up to now, no definite evidence for QPOs nor phase lags has been reported in AGNs, although multi-wavelength observations of some active galaxies seem to indicate a correlated variability between the optical-UV and X-ray fluxes (Clavel et al. (1992); Edelson et al. (1996); Nandra et al. (1998)). Time delays of a few days between the optical-UV and X-ray bands could be detectable, providing a powerful tool to probe the geom-

etry of the accretion flow in the nuclear regions, as recently suggested by Zampieri et al. (2000).

The analogies between the spectral properties in the optical/UV/X-ray bands and, possibly, the variability patterns in BHCs and AGNs suggest that in both classes of sources the same basic mechanism might be responsible for the observed emission. Much effort was devoted in recent years to envisage a "unified" scenario that has been partially successful in explaining the different spectral states in BHCs. The current picture is based on a two-component accretion flow: a standard disc and a hotter phase which could be advection-dominated (see e.g. Narayan, Mahadevan & Quataert (1999)). The different states are then produced by the varying importance of the two components. However, specific models do not provide a consistent description for the structure and evolution of the accretion flow.

It has been known since a long time that the inner regions of a standard disc are thermally and viscously unstable (e.g. Pringle, Rees & Pacholczyk (1973); Shapiro, Lightman & Eardely (1976); Ichimaru (1977)). This suggested the intriguing possibility that the observed spectral transitions may be triggered by such instabilities. A definite answer should be sought in terms of a time-dependent hydrodymical approach, such as that adopted by Honma, Matsumoto & Kato (1991) and Szuszkiewicz & Miller (1997), (1998). In particular, the latter authors have calculated the non-linear (global) evolution of transonic accretion discs produced by the onset of a thermal instability driven by radiation pressure and have shown that the evolution follows a cyclic pattern, passing through successive stages of evacuation and replenishment of the inner disc region (see also Takeuchi & Mineshige (1998)).

Ultimately, in order to get detailed theoretical predictions for the observed quantities, it is necessary to compute the spectra emitted during the instability cycle. Model spectra should properly take into account for the effects of the disc atmosphere, through which energy deposition is likely to take place at different heights. Models of disc atmospheres have been already presented (LaDous (1989); Shimura & Takahara (1993)) and some thought has been given to the problem of energy deposition (Shaviv & Wehrse (1986); Hubeny (1990)). The first thorough investigation of the vertical structure and emission spectrum of a thin accretion disc has been presented by Shimura & Takahara (1995), who found that, for intermediate accretion rates, local spectra, emitted from each disc annulus, can be approximated by a Planckian with an average hardening factor $f \sim 1.7$. Investigations of the spectra emitted by steady-state, dissipative accretion discs in AGNs have been carried out by Sincell & Krolik (1998) (standard discs) and Wang et al. (1999) (slim discs). Recently, Hubeny and co-workers ((2000) and references therein) reported on the progress in their long term programme to construct detailed spectra from stationary, thin accretion discs in AGNs.

In this paper we compute spectra under the slim-disc approximation, which is appropriate for modeling intrinsically bright sources and allows us to follow the non-stationary evolution of a disc subject to a thermal instability. We will assume that energy deposition takes place entirely in the disc. More complex situations in which energy deposition occurs also in the atmosphere will be considered in a follow-up paper. This work is part of an ongoing research programme dedicated to the analysis of hydrodynamical instabilities in slim accretion discs and to the modeling of the spectral and variability properties of BHCs, in particular of the microquasar GRS 1915+105. In this paper we compute the spectra that emerge from slim discs during their instability cycle and discuss their possible relevance for the soft spectral component of GRS 1915+105. The paper is organized as follows. In Section 2 we describe the structure and evolution of thermally unstable transonic disc, concentrating on those properties relevant to spectral calculations. In Section 3 our approach to the solution of radiative transfer in the disc atmosphere is outlined. Computed spectra are presented in Section 4. Discussion and conclusions follow in Section 5.

2 RADIAL STRUCTURE OF A THERMALLY UNSTABLE TRANSONIC ACCRETION DISC

Thermally unstable discs may undergo a limit-cycle behaviour with successive evacuation and refilling of their central parts. By means of a full time-dependent hydrodynamical simulation, Szuszkiewicz & Miller (1998) explored in detail a model with black hole mass $M = 10M_{\odot}$, initial accretion rate $\dot{M} = 0.96$ (in Eddington units) and viscosity parameter $\alpha = 0.1$. In this particular model the cycle has a duration of about 780 s and can be divided into two distinct parts: a very short ($\sim$ 20 s) outburst phase, during which the inner part of the disc is evacuated, and a quiescent stage (corresponding to the slow refilling) lasting for $\sim$ 760 s. We have chosen four particular snapshots during the disc evolution for which to calculate emergent spectra. They correspond to the end of the refilling phase, just before the outburst starts (model 1), the peak of the outburst (the maximal evacuation stage, model 2), the beginning (model 3), and half way through the refilling phase (model 4). The theoretical bolometric light curve together with the positions of the four chosen snapshots is shown in Fig. 1. In this section we discuss the radial structure of the disc for each of the four stages.

The electron temperature distributions for models 1-4 are shown in Fig. 2; unless stated otherwise, hereafter all lengths are in units of the Schwarzschild radius, $r_G = 2GM/c^2$. Before the instability sets in (model 1) the temperature profile is that given by the solid line, labeled 1 in Fig. 2. At the onset of the instability, two density waves are sent out from the locally-unstable region, one moving inwards and the other outwards. At the same time the temperature rises significantly in the unstable region. As the outgoing wave progresses the temperature peak is reduced (model 2) but remains still above that of model 1. Another effect of the propagating wave is to push a significant amount of matter outwards leaving behind an underdense region. This can be seen in Fig. 3 where the volume density is plotted against radius. The outgoing wave heats the material through which it passes, causing the perturbed part of the disc to swell up, as shown in Fig. 4. During the evacuation phase the disc temperature is high. However, once the wavefront has moved beyond the linearly unstable region, the disc cannot remain at such a high temperature for a very long time. Eventually the front weakens and the temperature falls dramatically

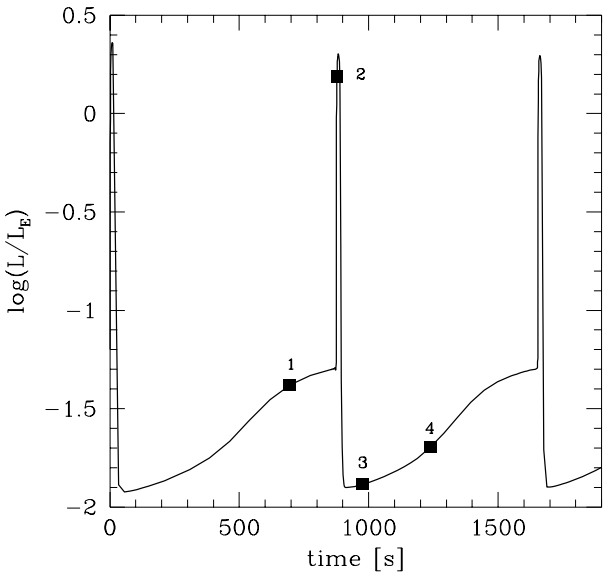

Figure 1. The bolometric light curve with the positions of four particular evolutionary stages described in the text.

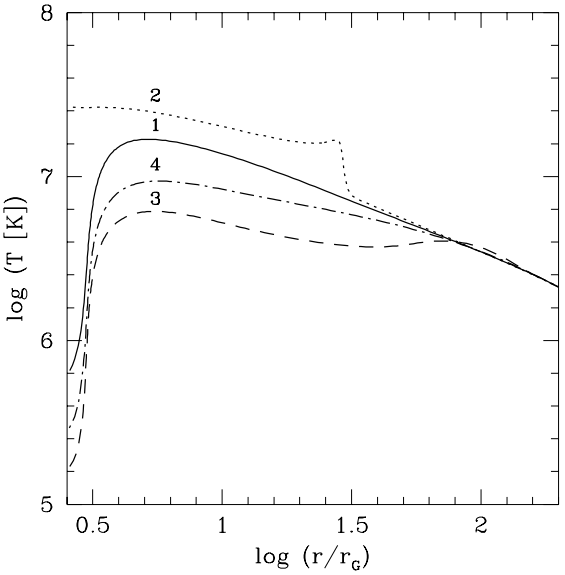

Figure 2. The radial profile of the midplane electron temperature for the four particular evolutionary stages discussed in the text.

(model 3). After this, the underdense region begins to fill up on a viscous time-scale. This increase in density is associated with a progressive rise in the temperature.

A quantity of immediate interest for spectral calculations is the effective optical thickness of the disc, $\tau_{eff} = [\tau_a(\tau_{es} + \tau_a)]^{1/2}$; here τ_{es} and τ_a are the scattering and absorption depths respectively. As shown in Fig 5, during the the maximal evacuation stage (model 2) the effective optical depth drops slightly below unity in the disc inner region. However, τ_{eff} is sufficiently large to safely assume that the radiation field in the disc is in LTE. Then, close to the equatorial plane the radiation intensity approaches a blackbody. In traversing the disc atmospheric layers radiation goes out of equilibrium and scattering effects are likely to change the

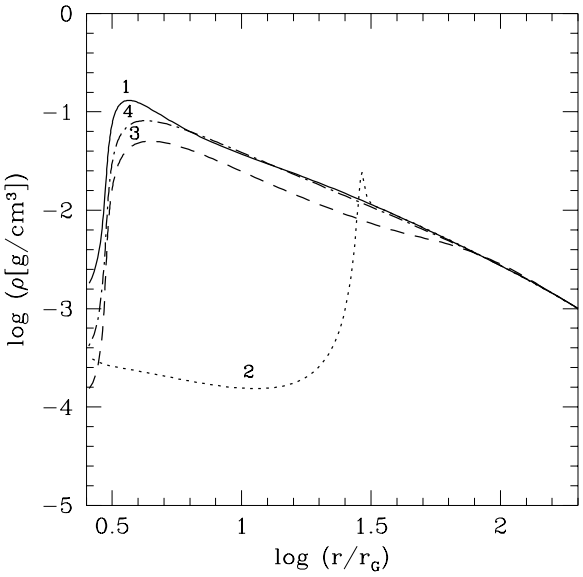

Figure 3. Same as in Fig. 2 for the volume density.

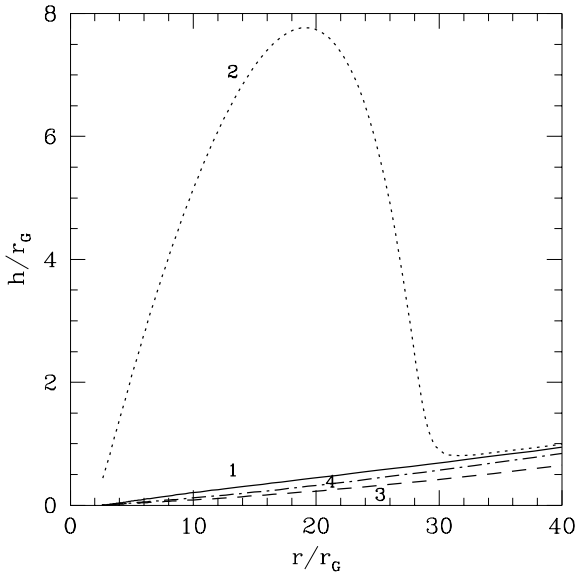

Figure 4. Same as in Fig. 2 for the disc half-thickness.

spectrum, as we will discuss in more detail in Section 4. The total flux distribution for each stage of the evolution is shown in Fig. 6. Neglecting relativistic effects, the total luminosity of the disc in the four different stages L_{disc} can be computed integrating the flux over the disc surface (see Table 1). It should be noted that L_{disc} becomes larger than the Eddington limit in the outburst phase. Super-Eddington luminosities may indeed be produced during the non-steady evolution and/or in a non-spherical flow. In this particular case, this happens because of the significant transient increase in the disc temperature. The flux together with the disc thickness will be used in the next section to calculate the emergent spectra.

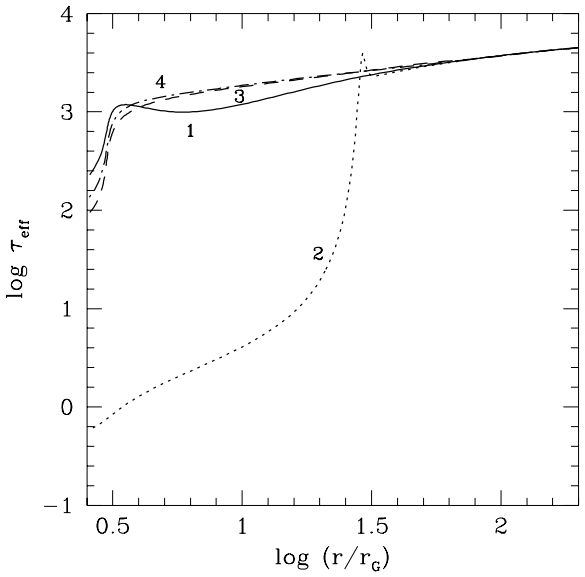

Figure 5. Same as in Fig. 2 for the effective optical depth.

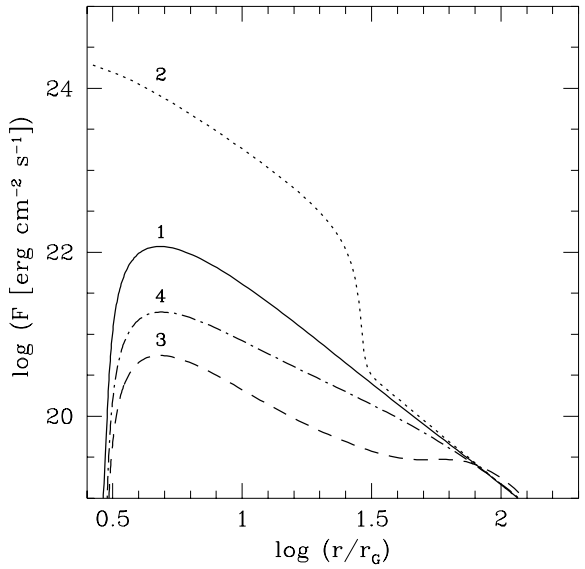

Figure 6. Same as in Fig. 2 for the emitted flux.

3 RADIATIVE TRANSFER IN THE DISC ATMOSPHERE

In this section we outline the numerical method used in computing the evolution of the radiation spectrum emitted by the transonic accretion disc. As discussed previously (see Section 2), we consider four stages that correspond to the maximal evacuation stage (model 2) and three replenishment stages (model 1, 3 and 4).

The radial grid of each numerical disc model is made up of ∼250 points dividing the integration domain, $r_{in} = 2.5 < r < r_{out} = 2.8 \times 10^5$, into a succession of comoving annular zones, each one 11% more massive than the one interior to it. The mass of the innermost zone was determined in accordance with numerical convenience. In order to compute the spectrum of these models, we introduce coarser radial zones (or rings) whose width is fixed by the requirement that their contribution to the total luminosity is $\sim 5\%$. We have found more convenient to keep the ring boundaries coincident with the mesh points of the hydrodynamic calculation, avoiding unnecessary interpolations. The luminosity L_r and average height h_r of each ring are then computed as

$$L_r = \sum_i 2\pi r_{i-1/2} \Delta r_i r_G^2 F_{i-1/2} \tag{1}$$

$$h_r = \sum_i h_i / N \tag{2}$$

where r_i and Δr_i are the radial mesh and grid spacing of the time-dependent hydrodynamic code, $F_{i-1/2}$ and $h_{i-1/2}$ are the radiative flux and disc height (evaluated at the midpoint) and N is the number of radial points within the ring. Clearly, since the ring luminosity is calculated as the sum of the contributions from the original zones, it differs slightly from one annulus to another. In terms of the width $\Delta r = r_N - r_1$ and the average radius $r_m = (r_1 + r_N)/2$ of each ring, the luminosity can be approximately written as

$$L_r = 2\pi r_m \Delta r r_G^2 \sum_i F_i / N \,. \tag{3}$$

We found that the aforementioned zoning procedure guarantees a sufficient accuracy when summing up all the rings and comparing the total disc luminosity to that computed from the output of the transfer calculation. However, especially in model 2, the temperature may change significantly within a ring and this contrasts the assumption, which will be introduced later on, that it may be approximated as isothermal. Therefore, we further ask that the fractional temperature variation in each ring does not exceed 2.5%, independently of the zone luminosity. Because the outermost zones of the original grid do not contribute appreciably to the total luminosity, they are grouped together into one single broad ring. Typically, this procedure results in a total number of rings $N_{rings} = 30 - 40$ (see table 1 for details).

The calculation of the radiation spectrum from each annulus proceeds in a way similar to that of Shimura & Takahara ((1993); (1995)) for Shakura-Sunyaev discs. Each ring is characterized by its luminosity and height above the mid-plane, and is approximated as (radially) isothermal. No energy dissipation occurs in the disc atmosphere that is then in radiative energy equilibrium. All the radiative flux is produced in the disc and enters the atmosphere from below. Consequently, the radiative luminosity is constant throughout the atmosphere, $L = L_r$.

The vertical structure is computed solving the coupled hydrostatic, energy and transfer equations in a plane-parallel, completely ionized, hydrogen layer. Solving the transfer of radiation in a geometrically thin *plane parallel* slab is formally very similar to solving the corresponding problem in a geometrically thin *radial* atmosphere. Thus we decided to model the disc atmosphere using the same equations considered by Zampieri et al. (1995) for a static, spherically symmetric, hydrogen atmosphere around a neutron star. The equations have been slightly modified neglecting general relativistic corrections, taking into account for the radial displacement of the ring from the center of gravity and suppressing the energy release within the atmosphere. The scattering depth $\tau = -\int_{h_r}^{\infty} \kappa_{es} \rho \, dz$ (here κ_{es} is the scat-

Table 1. Model parameters.

Model	L_{disc}/L_E	Radial zones	f_{ave}
1	4.8×10^{-2}	33	1.64
2	1.54	41	1.65
3	1.6×10^{-2}	29	1.65
4	2.4×10^{-2}	32	1.65

tering opacity and ρ the density) is used as the independent variable and the inner and outer boundaries are placed at $\tau_{in} = 8$ and $\tau_{out} = 10^{-4}$, respectively. The variation of the height $z(\tau)$ is obtained by differentiation. The radiation spectrum is computed from the first two moment equations for the monochromatic radiation energy density U_ν and flux F_ν, assuming that at the base of the atmosphere, where the $\tau_{eff} > 1$, the radiation field is Planckian. This set of coupled differential equations provides the run of pressure P, temperature T, height z, radiation energy density U_ν and flux F_ν as functions of depth. The density is obtained from the perfect gas equation of state. A thorough discussion of the numerical method adopted to solve these equations can be found in Nobili, Turolla & Zampieri (1993).

We note that the luminosity computed by the transfer code is $L_{r,sph} = 4\pi r_{sph}^2 r_G^2 \int F_\nu d\nu$, where r_{sph} is an "effective spherical radius". Assuming $\int F_\nu d\nu = \sum_i F_i/N$ and $L_{r,sph} = L_r$ (equation [3]), we obtain

$$r_{sph} = \sqrt{r_m \Delta r/2}\,. \tag{4}$$

The spectrum emitted by the whole disc is evaluated by summing up the contributions from the various rings

$$L_{\nu,disc} = \sum_{rings} 4\pi r_{sph}^2 r_G^2 F_\nu\,. \tag{5}$$

4 SPECTRA FROM TRANSONIC ACCRETION DISCS

Local spectra from a number of selected radial zones are shown in Figs. 7 and 8 for the four evolutionary stages considered, together with the corresponding temperature profiles in the disc atmosphere. We found that the emergent spectra are harder than the blackbody at the ring effective temperature, $T_{eff,r} = (L_r/2\pi r_m r_G^2 \Delta r \sigma)^{1/4}$ (here σ is the Stefan-Boltzmann constant). The presence of an overall spectral hardening is a common feature of radiative transfer in plane-parallel atmospheres and has been discussed by various authors in different contexts (e.g. London, Howard & Taam (1986) for atmospheres around X-ray bursting neutron stars; Romani (1987) and Zampieri et al. (1995) for atmospheres around cooling and accreting neutron stars; Shimura & Takahara (1995) for the reprocessing of radiation by the top layers of Shakura-Sunyaev discs).

The hardening is essentially caused by two distinct effects. Models 1, 3 and 4 have an average $\dot{M} \sim 0.5$ (in Eddington units) and are rather cool (atmospheric temperature $\lesssim 5{\times}10^6$ K). Their deeper layers ($\tau \sim \tau_{in}$) are comparatively hotter, $T(\tau_{in}) \gtrsim T_{eff}$. High energy photons produced there escape more easily, because the free-free opacity (which is the main source of absorption) declines rapidly with increasing frequency. The emergent spectrum is then, roughly, the superposition of blackbody spectra with decreasing temperatures, which is peaked at $\approx kT(\tau_{in})$. This mechanism is responsible for the spectral broadening with respect to a Planckian and the sensible deviation from the best-fitting blackbody in the local spectra of models 1, 3 and 4 (see Fig. 8 and the upper left panel in Fig. 7).

The case is different for model 2, which is more luminous and comparatively hotter, $T(\tau_{in}) \lesssim 3 \times 10^7$ K, with an average accretion rate $\dot{M} \sim 25$ (in Eddington units). Local spectra at small radii are more affected by scattering and they appear nearly Planckian close to the maximum. The scattering depth of the inner layers ($\tau_{in} \sim 10$) is large enough to build up a Compton parameter $y = 4(kT/mc^2)\max(\tau, \tau^2) \sim 0.1 - 1$. Therefore, high energy photons tend to fill the Wien peak at the local atmospheric temperature and photons with energy $\gtrsim 3kT$ are systematically downscattered. As Shimura & Takahara (1995) pointed out, this explains the nearly Planckian shape of the spectrum close to the maximum and also the low energy tail in excess to the best-fitting blackbody clearly visible in the first three spectra in Fig. 7 for model 2. The Compton parameter of models 1, 3 and 4 is a factor ~ 10 smaller, $y \lesssim 0.1$, not large enough to produce any spectral distortion.

Despite the fact that local spectra may deviate appreciably from a blackbody, it is quite useful to introduce, as is commonly done, a hardening factor to quantify the spectral changes caused by radiative transfer in the disc atmosphere. For each radial zone the fit of the computed spectrum with a Planckian, $\propto \nu^3/(\exp h\nu/kT_c - 1)$, gives the color temperature T_c. The hardening factor is defined as $f = T_c/T_{eff}$ and measures the overall energy shift of the spectrum with respect to the blackbody at T_{eff}, regardless of the actual spectral distortions. The run of the hardening factor in the disc is shown in Fig. 9. Quite remarkably, we find that the hardening factor is very similar in all four evolutionary stages considered here, and is very nearly constant through the disc. The typical value is $f \sim 1.65$ and it shows only a marginal increase in the outer zones. Following Shimura & Takahara (1995), we define a radially-averaged hardening factor as

$$f_{ave} = \sum_{rings} f_r/N_{rings}\,. \tag{6}$$

The values of f_{ave} for our models are listed in table 1 and the spectra from the whole disc are shown in Fig. 10, together with the multicolor blackbody spectra at fT_{eff} with both $f = f_{ave}$ and $f = 1$. As shown in Fig. 10, with the possible exception of the intermediate energy range of model 2, the spectrum from the whole disc can be qualitatively described in terms of a superposition of Planckian spectra with an average temperature calculated using f_{ave}. We note that a similar result was found by Shimura & Takahara (1995) for Shakura-Sunyaev discs with intermediate values of the accretion rate and $\alpha = 0.1$.

The behavior of the hydrodynamic variables across the disc atmosphere is briefly illustrated here. Because the luminosity of each radial zone is well below the Eddington limit, pressure scales linearly with depth. The temperature variation across the atmosphere is rather modest: T decreases monotonically outwards, with the exception of the inner zones of model 2, where the increase is caused by the effectiveness of Compton heating/cooling in the energy balance (see the bottom panels in Figs. 7-8). The atmospheric scale

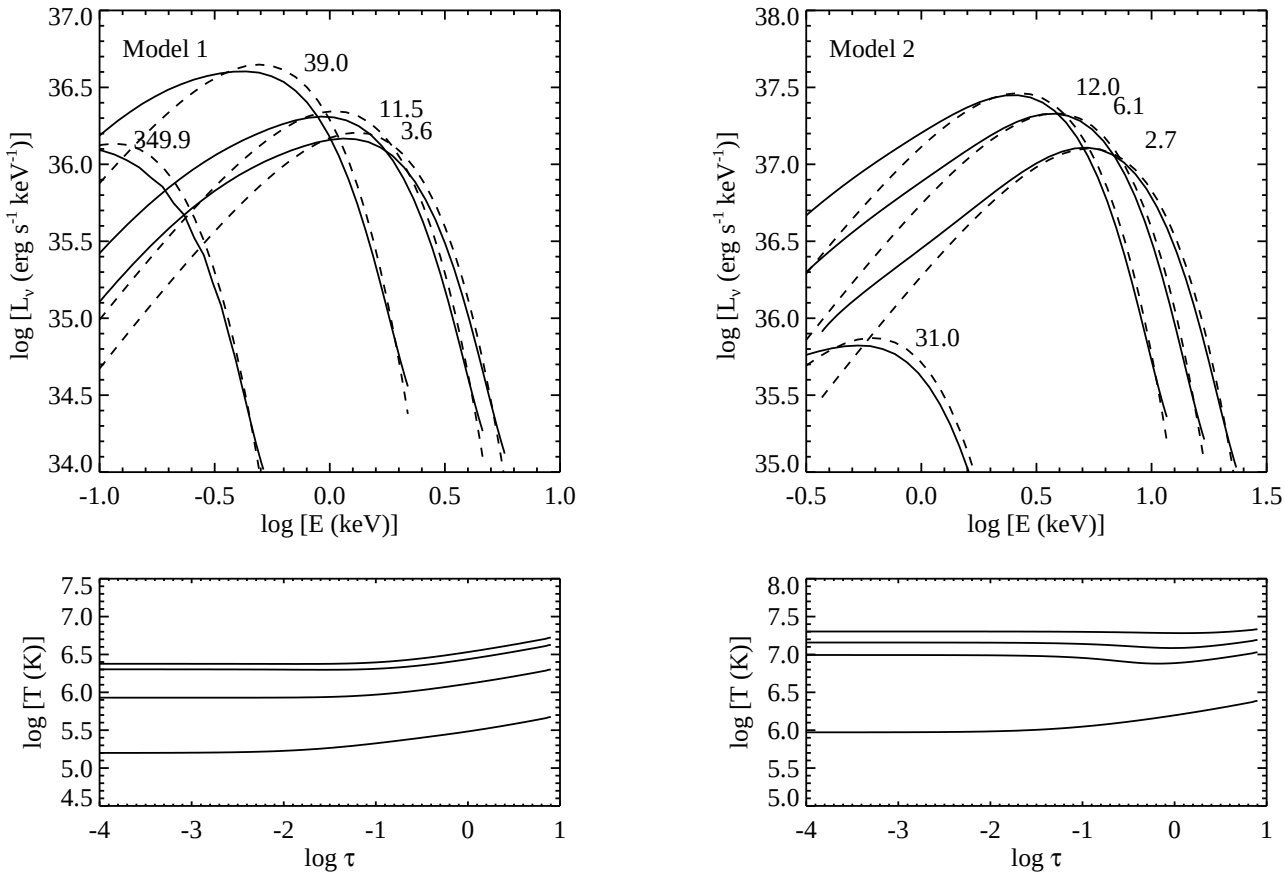

Figure 7. Upper panel: local spectra at different radii (full lines) together with the best-fitting blackbody (dashed lines) for model 1 (left) and model 2 (right); lower panel: the run of temperature in the atmosphere vs. scattering depth.

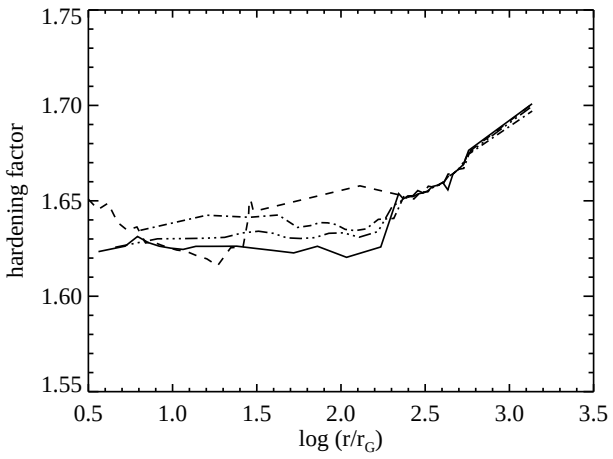

Figure 9. The radial variation of the hardening factor for models 1-4 (full, dash, dash-dotted, dash-double dotted line respectively).

height is always quite small and the fractional increase of $z(\tau_{out})$ over the average ring height h_r is only a few percent.

Although present spectra can not be taken as representative of the whole X-ray emission from BHCs, in that they do not exhibit any power-law hard tail (see section 5), actual spectra as seen by an observer at infinity have been calculated. General relativistic effects have been included, following the method by Cunningham (1975). We consider here only the case of a Schwarzschild black hole, to which the pseudo-Newtonian potential is the closest non-relativistic analog. The same calculation could be easily performed for a maximally rotating Kerr black hole but this seems not appropriate in the present framework. The original assumption of Keplerian rotation has been maintained. Deviations from a pure Keplerian law in our disc models are not too large and should not introduce major differences. The specific intensity at the top of the atmosphere ($\tau_{out} = 10^{-4}$), needed to evaluate Cunningham's expression for the luminosity at infinity, has been obtained in terms of the first two moments of the radiation field as

$$4\pi I_\nu(\mu) = cU_\nu + 3\mu F_\nu = (2 + 3\mu)F_\nu \qquad (7)$$

where ν is the frequency measured by a local observer comoving with the disc and $\mu = \cos\theta$. Results are shown in Fig. 11 for different viewing angles, θ. Apart the obvious decrease in amplitude produced by inclination and gravitational effects, two major features are apparent in the spectra at infinity, particularly in the high energy tail which is produced deeper into the potential well. First, the exponential cut-off is shifted to lower energies with respect to the Newtonian model because of the gravitational redshift and, second, the spectrum tends to become harder for increasing inclination angle. This is because the orbital motion acquires a larger component along the line-of-sight and this produces a

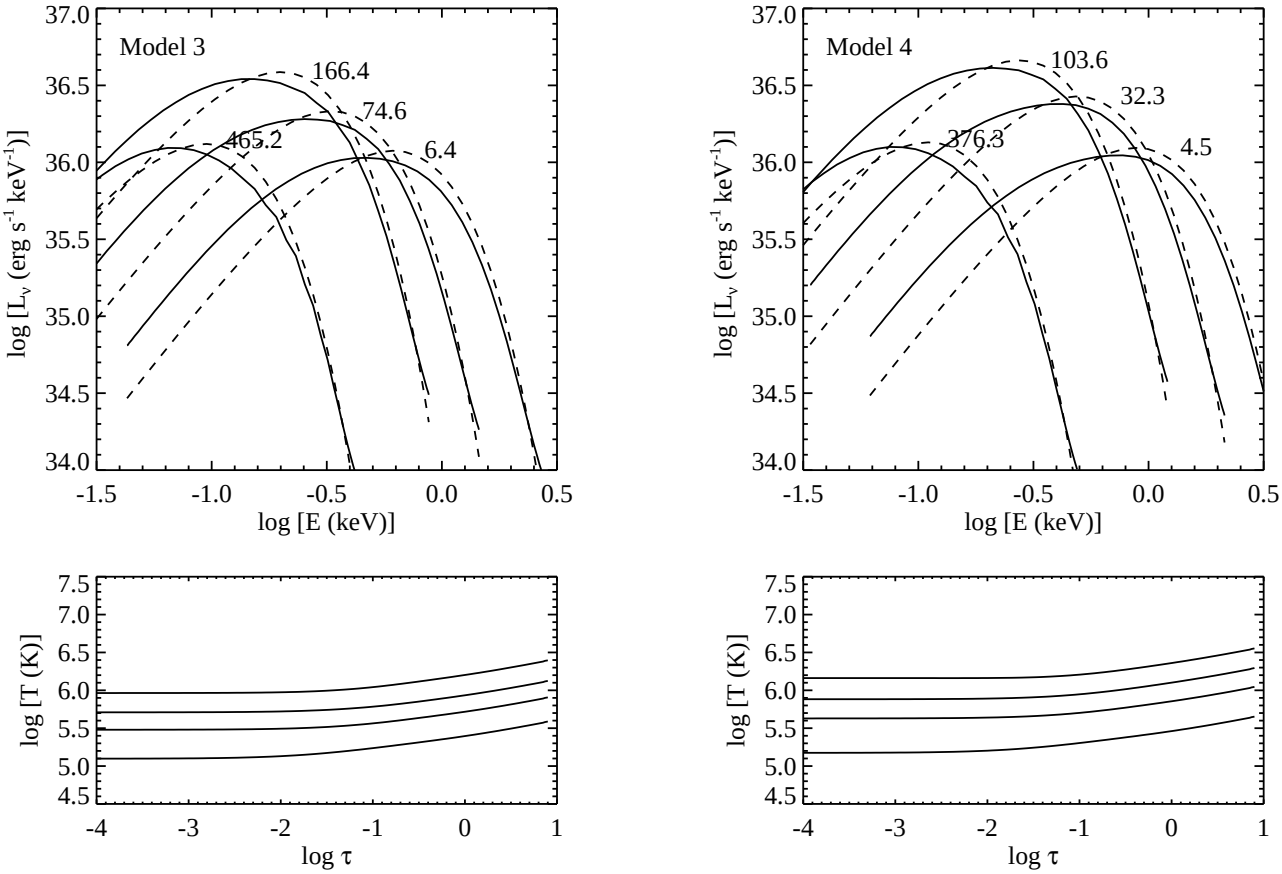

Figure 8. Same as in Fig. 7 for model 3 (left) and model 4 (right).

larger kinematical blue-shift. Finally, we note that owing to relativistic ray-bending, radiation from the inner zone can be seen also when the disc is edge-on ($\cos\theta = 0$).

5 DISCUSSION AND CONCLUSIONS

In this paper we have investigated the emission properties of time-dependent, slim accretion discs, calculating for the first time the evolution of the disc spectra along the limit instability cycle. This work is part of an ongoing numerical programme to investigate the time-dependent behaviour triggered by the onset of various types of instability (thermal, viscous and acoustic), as outlined in Szuszkiewicz & Miller (1997), and to get detailed theoretical predictions for observational quantities relevant to accreting black holes in galactic X-ray binaries and AGNs, as outlined in Szuszkiewicz, Turolla & Zampieri (2000).

Away from the outburst (maximal evacuation) phase, the spectrum emitted by each annulus of the disc deviates significantly from a pure Planckian distribution, showing a characteristic broadening. This effect is typical of the spectra emitted by free-free dominated atmospheres and is caused by the superposition of photons emitted at different depths: because of the energy dependence of the free-free opacity, more energetic photons are emitted in the deeper atmospheric layers, where the temperature is higher. Outburst spectra are more Planckian in shape around the maximum because the higher atmospheric temperature makes comptonization comparatively more effective: photons tend to form an excess at low energies and to fill the Wien peak at high energies. A usual way to estimate the overall hardening of a thermal spectrum is to compare the best-fitting Planckian distribution with a blackbody at the effective temperature. We found that, in all stages of the instability cycle, the temperature of the best-fitting blackbody is typically larger than the local effective temperature by a factor $f \sim 1.65$, indicating that the hardening factor is substantially constant both in radius and time. There is only a slight increase of f with radius in the outer region. Therefore, although the mechanism responsible for the hardening is different (thermal comptonization in one case and superposition of blackbody spectra in the others), outburst spectra have an average hardening factor comparable to that of the spectra emitted during the evacuation and refilling stages. We note that the average value of the hardening factor for the local spectra in the initial state and the tendency to increase outwards are consistent with what found for a Shakura-Sunyaev disc by Shimura & Takahara ((1995); $f \sim 1.7$) for similar values of the black hole mass, viscosity parameter and accretion rate. The values of the hardening factor during the other stages cannot be directly compared because the structure of the disc is rather different.

In this investigation we focused on the properties of radiation emitted by thermally-unstable accretion discs. We

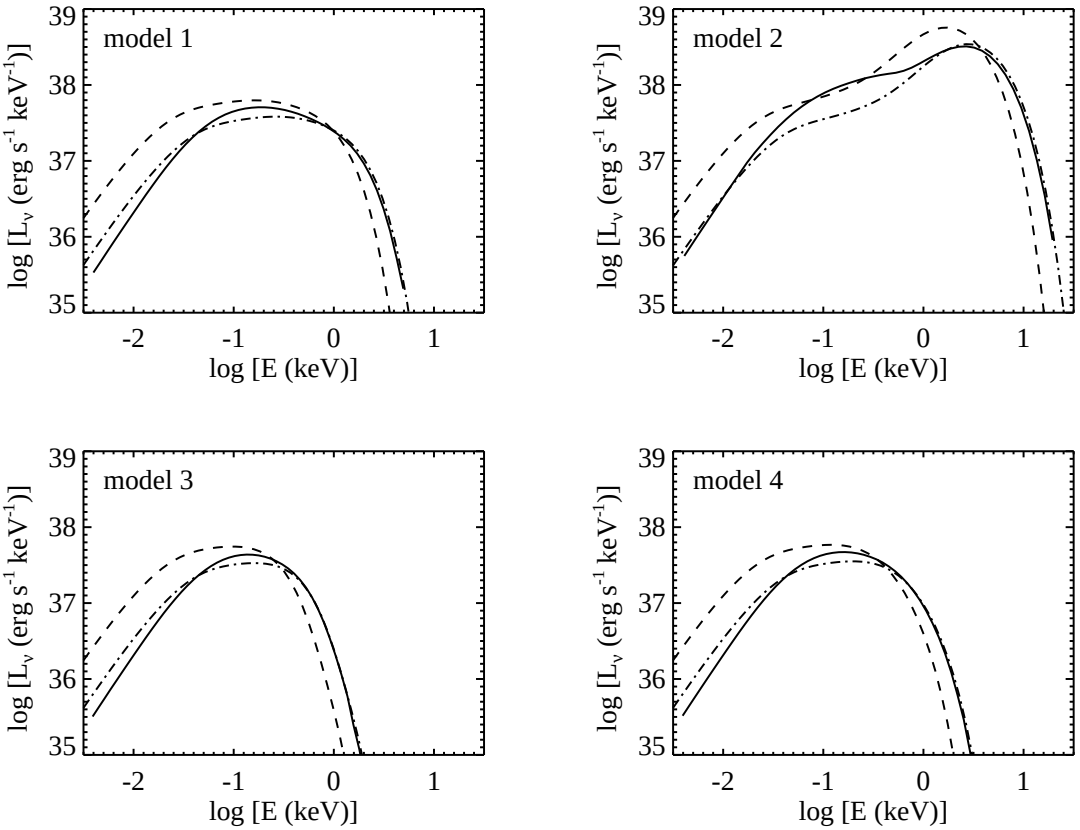

Figure 10. Spectra emitted by the whole disc (full lines) together with the multicolour blackbody spectra at T_{eff} (dashed lines) and at $f_{ave}T_{eff}$ (dash-dotted lines).

remind that in the present model no energy is released in the disc atmosphere and that no high-energy, thermal or non-thermal, electron component has been included. Therefore, computed spectra are thermal and do not show the hard tail often observed in BHCs and AGNs. This must be taken into account in comparing present models with the observed spectra, in that only the evolution of the soft component can be reproduced. As shown in Figs. 10 and 11, our model undergoes rather dramatic spectral changes along the instability cycle. The spectrum emitted before the instability sets in is typical of a standard accretion disc at moderate accretion rates and has a broad bump in the 0.1–1 keV band. During the outburst phase, the inner region becomes hotter and contributes most of the high energy emission in the 1–10 keV range: a very pronounced peak, centered around $\sim$ 5 keV appears in the spectrum. The spectrum then softens considerably during the refilling phase, up to the point that almost no photons are emitted above $\sim$ 1 keV. A usual way to describe the observed spectra, frequently used in X-ray astronomy at low energy resolution, is to compute the hardness ratios. Because present spectra lack the power-law, high energy tail, we do not attempt to make a quantitative comparison with the observed hardness ratios but simply track their evolution during the cycle. In Table 2 we report the hardness ratio HR1 (HR2), defined as the ratio of the count rate in the 5-13 (13-60) keV energy band over the count rate in the 2-5 keV band, for the computed spectra of models 1 and 2 (the values for model 3 and 4 are zero). The calculation has been performed using the RXTE response function and accounting for interstellar absorption (with a column density $N_H = 2 \times 10^{22}$ cm^{-2}). As shown in Table 2, the hardness ratios at the beginning of the cycle are low. However, during outburst they increase reaching interesting values (HR1 $\sim$ 1, HR2 $\sim$ 0.03). Table 2 clearly indicates that the evolution of our model along the instability cycle is qualitatively very similar to the evolution of the soft component in GRS1915+105 (see Belloni et al. (2000)). In this respect, it is tempting to interpret the observed soft state B (characterized by a higher temperature) as corresponding to the outburst spectral state of our models. The higher temperature is associated to the innermost part of the disc, accreting at much higher rates than the outer unperturbed part. Further investigation of this promising result is definitely required and is presently under way.

A few comments on the assumptions involved in our treatment of the accretion flow and radiative transfer should be made. We decided to use the slim disc approximation even if we are aware that realistic discs are truly 2D structures in which all thermodynamic quantities vary with height and radius. Modeling the 2D structure of accretion discs is much more complicated than using a 1D vertically averaged approximation. However, as recently discussed by Huré & Galliano (2001), the accuracy of vertically averaged models should be sufficient in practice for many astrophysical appli-

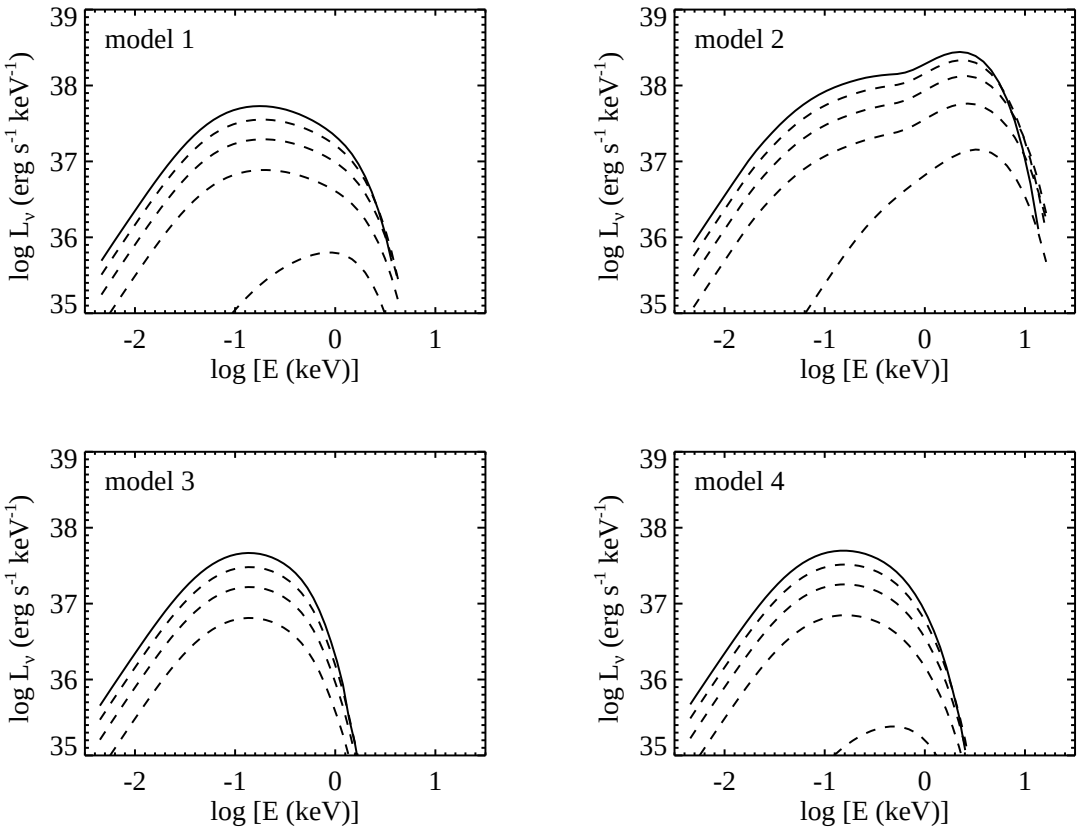

Figure 11. Observed spectra at radial infinity for different viewing angles. The full lines refer to $\cos\theta = 1$ (disc face-on), whereas the dashed lines show spectra observed at $\cos\theta = 0.75, 0.5, 0.25, 0$ (from top to bottom).

Table 2. Hardness ratios for the computed spectra of models 1 and 2.

	model 1		model 2	
$\cos\theta$	HR1[a]	HR2[b]	HR1[a]	HR2[b]
1	0.021	0	0.63	0.003
0.75	0.042	0	0.83	0.014
0.5	0.055	0	1.02	0.031
0.25	0.064	0	1.18	0.052
0	0.05	0	1.31	0.054

[a] HR1 = (5-10 keV)/(2-5 keV).
[b] HR2 = (13-60 keV)/(2-5 keV).

cations. The slim disc model (Abramowicz et al. (1988)) retains the assumption that the disc is geometrically thin but the centrifugal force no longer balances gravity exactly. The thickness of the disc depends on both pressure and viscosity: the higher is the pressure and (in general) the viscosity, the thicker is the disc. In going from extremely thin discs to thicker ones, the effects of advection become progressively more important. The slim disc approach includes the effects of advection in a correct way while continuing to make use of vertical averaging. Advection is particularly important for the inner parts of an accretion disc around a black hole: while a standard Keplerian disc ends at the marginally stable orbit, a realistic accretion flow may continue inwards and must cross a sonic point before reaching the event horizon. Finally, we note that gravity has been represented by the pseudo-Newtonian potential of Paczyński & Wiita (1980), which describes in a satisfactory way the dynamical effects of the Schwarzschild gravitational potential. The main approximation that has been introduced in treating the vertical transfer of radiation in the disc concerns stationarity. This approximation turns out to be very good almost everywhere in the disc because the time-scale over which the radiation field changes is much shorter than the fastest dynamical time r/v_ϕ, $t_{rad} = (c_s/c\tau_{eff})(r/v_\phi) \ll r/v_\phi \ll r/v_r$, where c_s, v_ϕ and v_r are the sound, azimuthal and radial velocities. Only in the transonic region of the disc this approximation might break down. However, the radial extent of this region is usually fairly small and does not contribute significantly to the total disc luminosity ($\lesssim 5\%$ for the outburst state). The disc model used here neglects all the effects induced on the surface layers by the X-ray photons produced (or scattered) by an external medium. X-ray illumination by an external source heats the disc photosphere and leads to the formation of a highly ionized layer which can become Thomson thick for large enough luminosities (see e.g. Nayakshin, Kazanas & Kallman (2000); Nayakshin & Kallman (2001)). While this will definitely influence the emitted spectrum shifting the emission at higher energies, its effect onto the hardening

factor are more difficult to estimate and would require a consistent calculation. We only note that present results show that f is not much sensitive to the disc surface temperature (see Table 1).

ACKNOWLEDGMENTS

E.S. gratefully acknowledges financial support from the Polish State Committee for Scientific Research (grant KBN 2P03D01817), the Italian Ministry for University and Scientific Research (MURST) and the University of Padova. Work partially supported by MURST through grant COFIN-98-02154100.

REFERENCES

Abramowicz M.A., Czerny B., Lasota J.-P., Szuszkiewicz E., 1988, ApJ, 332, 646
Belloni T., et al., 1997, ApJ, 479, L145
Belloni T., et al., 2000, A&A, 355, 271
Clavel J., et al., 1992, ApJ, 393, 113
Cui W., 1999, ApJ, 524, L59
Cui W., Zhang S.N., Chen W., 2000, ApJ, 531, L45
Cunningham C.T. 1975, ApJ, 202, 788
Edelson R.A., et al., 1996, ApJ, 470, 364
Grebenev S.A., et al., 1993, A&AS, 97, 281
Grebenev S.A., Sunyaev R.A., Pavlinsky M.N., 1997, AdSpR 19, 15
Honma F., Matsumoto R., Kato S., 1991, PASJ, 43, 147
Hubeny I., 1990, ApJ, 351, 632
Hubeny I., Agol E., Blaes O., Krolik J.H., 2000, ApJ, 533, 710
Huré J.-M., Galliano F., 2001, A&A, 366, 359
Ichimaru S., 1977, ApJ, 214, 840
La Dous C., 1989, A&A, 211, 131
London R.A., Howard W.M., Taam R.E., 1987, ApJ, 306, 170
Nandra K., et al., 1998, ApJ, 505, 594
Narayan R., Mahadevan R., Quataert E., 1999, in Abramowicz M.A., Bjornsson G., Pringle J.E., eds, The Theory of Black Hole Accretion Disks, Cambridge University Press, Cambridge
Nayakshin S., Kazanas D., Kallman T.R., 2000, ApJ, 537, 833
Nayakshin S., Kallman T.R., 2001, ApJ, 546, 406
Nobili L., Turolla R., Zampieri L., 1993, ApJ, 404, 686
Paczyński B., Wiita P., 1980, A&A, 88, 23
Pottschmidt K., et al., 2000, A&A, 357, L17
Pringle J.E., Rees M.J., Pacholczyk A.G., 1973, A&A 29, 179
Reig P., et al., 2000, ApJ, 541, 883
Romani R., 1987, ApJ, 313, 718
Shaviv G., Wehrse R., 1986, A&A, 159, L5
Shimura T., Takahara, F., 1993, ApJ, 419, 78
Shimura T., Takahara, F., 1995, ApJ, 445, 780
Shapiro S.L., Lightman A.P., Eardley D.M., 1976, ApJ, 204, 187
Sincell, M.W., Krolik, J.H., 1998, ApJ, 496, 737
Szuszkiewicz E., Miller J.C., 1997, MNRAS, 287, 165
Szuszkiewicz E., Miller J.C., 1998, MNRAS, 298, 888
Szuszkiewicz E., Turolla R., Zampieri L., 2000, in Castro-Tirado A.J., Greiner J., Paredes J.M., eds, Granada Workshop on Galactic Relativistic Jet Sources, Ap&SS, in press
Takeuchi M., Mineshige S., 1998, ApJ, 505, L19
Tanaka Y., Lewin W.H.G., 1995, in Lewin W.H.G, van Paradijs J., van den Heuvel E.P.J., eds, X-Ray Binaries, Cambridge University Press, Cambridge
Wang, J.-M., Szuszkiewicz, E., Lu, F.-J., Zhou, Y.-Y., 1999, ApJ, 522, 839
Zampieri L., Turolla R., Zane S., Treves A., 1995, ApJ, 439, 849
Zampieri L., Nobili L., Turolla R., Belloni T., 2000, in Proc. 4th Italian AGN Conf., Mem.SAIT, in press
Zdziarski A.A., Gierlinski M., Gondek D., Magdziarz P., 1996, A&AS, 120, 553
Zdziarski A.A., Lubiński P., Smith D.A., 1999, MNRAS, 303, L11